Science of the Total Environment 859 (2023) 160311

Contents lists available at ScienceDirect

Science of the Total Environment

journal homepage: www.elsevier.com/locate/scitotenv

A new bi-radical species formed during the photochemical degradation of synthetic musk tonalide in water: Study of *in-situ* laser flash photolysis and validation of synthesized standard sample

Na Luo [a,b], Yanpeng Gao [a,b], Mei Wang [a,b], Xiaolin Niu [a,b], Guiying Li [a,b], Taicheng An [a,b,*]

[a] Guangdong-Hong Kong-Macao Joint Laboratory for Contaminants Exposure and Health, Guangdong Key Laboratory of Environmental Catalysis and Health Risk Control, Institute of Environmental Health and Pollution Control, Guangdong University of Technology, Guangzhou 510006, China

[b] Guangzhou Key Laboratory of Environmental Catalysis and Pollution Control, Key Laboratory of City Cluster Environmental Safety and Green development of the Ministry of Education, School of Environmental Science and Engineering, Guangdong University of Technology, Guangzhou 510006, China

HIGHLIGHTS

- Rapid photolysis of tonalide was observed with apparent rate constant of 0.24 min^{-1}.
- New bi-radicals generated from intramolecular H-abstraction verified by *in-situ* LFP.
- Products were identified by HPLC-Q-TOF and validated with synthesized standards.
- Photolysis mechanism of tonalide is the photoenolization followed the cyclization.
- Bioconcentration factor of photoenol was 13-fold higher than that of tonalide.

GRAPHICAL ABSTRACT

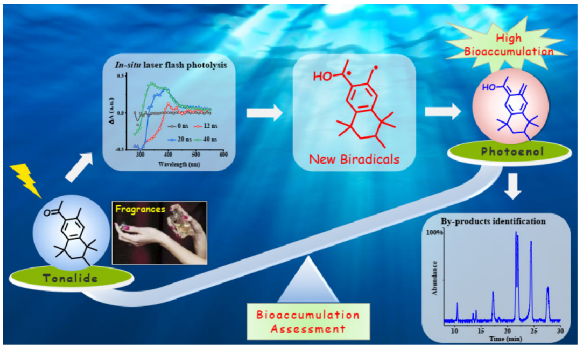

ARTICLE INFO

Editor: Jay Gan

Keywords:
Tonalide
Bi-radical formation
Photoenolization
Laser flash photolysis
Photochemical degradation mechanism

ABSTRACT

The ubiquitous presence of synthetic musks is causing serious concern due to the species produced from their transformation and environmental impacts. In this study, tonalide was selected as a representative synthetic musk to evaluate the transformation mechanism and pathway in water under ultraviolet (UV) irradiation. The results showed that tonalide could undergo rapid photochemical degradation through a new pivotal bi-radical, which acts as the initial active species. The bi-radicals with a typical absorption peak at 340 nm was observed by *in-situ* laser flash photolysis technology, and the absolute decay rate constant was obtained as $3.61 \pm 0.01 \times 10^9\ M^{-1}\ s^{-1}$ with the life-time of 83.3 ns. The photochemical degradation by-products of tonalide were also identified by high-performance liquid chromatography coupled with quadrupole time-of-flight mass spectrometry, and the precise structures of key by-products have been validated by our preparative synthesized standard samples confirmed by nuclear magnetic resonance. Thus, the mechanism of tonalide photochemical degradation, continuous photoenolization of the bi-radicals and followed cycloaddition reaction with O_2, was proposed as the predominant pathway. The main degradation by-product, photoenol which has a higher bioconcentration than that of tonalide, was found to form from the bi-radicals photoenolization. This study is the first work to propose a new bi-radical as the photoenol precursors during photochemical degradation of tonalide in water.

* Corresponding author at: Guangdong-Hong Kong-Macao Joint Laboratory for Contaminants Exposure and Health, Guangdong Key Laboratory of Environmental Catalysis and Health Risk Control, Institute of Environmental Health and Pollution Control, Guangdong University of Technology, Guangzhou 510006, China.
E-mail address: antc99@gdut.edu.cn (T. An).

http://dx.doi.org/10.1016/j.scitotenv.2022.160311
Received 26 September 2022; Received in revised form 15 November 2022; Accepted 15 November 2022
Available online xxxx

1. Introduction

Due to the widespread existence of emerging organic contaminants (EOCs) and products from their photochemical degradation in water, these have attracted more attention due to their environmental behaviors and adverse effects on human health (Vione and Carena, 2020). Generally, photochemical degradation is a pivotal pathway for the environmental geochemistry processes, and affects the environmental fate and transport of EOCs (Wang et al., 2021). In particular, EOCs could be transformed into various products during photochemical degradation, and potentially cause an increased adverse impact on aquatic ecosystem and human health (Gao et al., 2021). Due to the lack of products standards, the study focusing on the formation mechanisms of various products is always full of challenges (Jiang et al., 2021), thus further leading to a massive gap in the toxicology of by-products. Therefore, it is urgent to study the formation mechanism and recognition technology (such as high-resolution mass spectroscopy and nuclear magnetic resonance) of these abundant photochemical degradation products.

Synthetic musks (SMs) are common fragrance ingredients, and have been extensively used in a variety of scented personal care products such as perfumes, cosmetics, soaps, detergents and other daily cleaning products (Montes-Grajales et al., 2017; Reiner and Kannan, 2006). With the continuous improvement in the living standards, the demand for these scented consumer goods has grown (Li et al., 2018b). It has been estimated that the global use of these scented consumer goods is as high as 10,000 tons (Liu et al., 2020). As a result, SMs are released into the environment during the production, transportation, usage and treatment of these consumer goods and solid wastes, and therefore, have become a frequently detected contaminant in wastewater, surface water and sediments. For instance, SMs concentrations were up to 920–2160 $ng{\cdot}L^{-1}$ in the effluents after the treatment at sewage treatment plants in the USA (Sun et al., 2014a). Their concentrations in surface water lied within the range of 5.9–120.6 $ng{\cdot}L^{-1}$ in China (Hu et al., 2011), 150–16,720 $ng{\cdot}L^{-1}$ in South Korea (Lee et al., 2010), and 0.55–1739.42 $ng{\cdot}L^{-1}$ in Italy (Villa et al., 2012). Moreover, SMs have also been found in human tissues (Moon et al., 2012), breast milk of women (Zhang et al., 2015), and serum of exposed and general populations (Liu et al., 2013). Recent research suggested that SMs were bio-accumulative, genotoxic, endocrine-disrupting and carcinogenic compounds (Parolini et al., 2015; Yamauchi et al., 2008; Zhang et al., 2017), and had the potential adverse effects on aquatic organisms and human health (Liu et al., 2020).

Photochemical degradation is a pivotal pathway for aquatic environmental transformation and fate of many EOCs including SMs (Wang et al., 2015). Recent studies have shown that SMs can undergo rapid photochemical degradation under ultraviolet (UV) irradiation (Godayol et al., 2015), UV-induced oxidation of hydroxyl radicals (Santiago-Morales et al., 2012), and chlorine-containing UV irradiation (Wang and Liu, 2019). It is important to note that a few SMs are very sensitive to UV-induced photochemical degradation. For example, the degradation efficiency of polycyclic musk tonalide, which is one of the highly used synthetic musks, is up to 90 % in 15 min under UV irradiation (Santiago-Morales et al., 2012). Moreover, under UV irradiation, the rate of photodegradation of tonalide was approximately 12–30 times higher than polycyclic musk galaxolide (Sanchez-Prado et al., 2004). Therefore, tonalide could be a representative for studying the photochemical degradation of SMs under UV irradiation. Remarkably, these degradation processes have led to the formation of products resulting from the degradation of SMs, such as the formation of hydroxylation and aldehyde products in the hydroxy-mediated degradation of tonalide (Fang et al., 2017). However, the main purpose of these studies is to develop effective elimination techniques for SMs. There are few reports focusing on the degradation mechanism and the identification of transformation products of SMs. Comprehensive identification of these transformation products is still necessary yet challenging for developing a better understanding of the structures and formation mechanisms of these products due to the lack of standard samples of many degradation by-products (Kliegman et al., 2013).

In this work, the photochemical transformation kinetics, their mechanisms and final fate of SMs were investigated in detail by employing tonalide as the model SMs. Firstly, the photochemical degradation kinetics of tonalide was studied in aqueous solution. Then, the specific scavenging experiments and electron paramagnetic resonance experiments (EPR) were used to recognize the key reactive species involved in the photochemical degradation of this system. Meanwhile, *in-situ* laser flash photolysis technology was employed to investigate the degradation kinetics, analyze the transient intermediates, and monitor the decay of produced by-products. Furthermore, absolute rate constant was also obtained from the growth of transient intermediates. The photochemical degradation mechanism of tonalide was proposed based on the identified by-products using high-performance liquid chromatography quadrupole-time of flight tandem mass spectrometry (HPLC-Q-TOF-MS) and validated by synthesized standard samples using nuclear magnetic resonance spectroscopy (NMR). Finally, the bio-accumulation risk of tonalide and its photochemical degradation by-products were estimated using theoretical calculations. The results of the present study could provide more convincing information to better understand the environmental behavior and fate of tonalide in the aquatic environment.

2. Experimental

2.1. Chemicals and reagents

Ultrapure water (18.25 MΩ·cm) was used in all the experiments. All reagents and solvents were used as received. Tonalide (7-acetyl-1,1,3,4,4,6-hexamethyl-tetrahydronaphtalene; ≥98 % pure) was purchased from Adamas Reagent Ltd., China. Text S1 in the Supporting Information (SI) summarizes all other chemicals used in this work.

2.2. Photochemical kinetics and laser flash photolysis experiments

2.2.1. Photochemical degradation experiments

The photochemical degradation experiments were carried out in a photochemical reaction apparatus with 110 W high-pressure mercury lamp (BL-GHX-V, Shanghai Belang Instrument Co., Ltd., China) as the irradiation light source. The average irradiation intensity was around 22 $mW{\cdot}cm^{-2}$. The external circulating condensed water could keep the reaction temperature constant at 20 °C. The photochemical degradation of tonalide was performed on 30 mL of tonalide (500 μM) dissolved in acetonitrile (ACN) and water (1:1), and the mixture was evenly stirred to ensure a uniform solution. Samples of approximately 1 mL volume were collected at a certain time interval, and analyzed using high-performance liquid chromatography (Agilent 1260 HPLC) with isocratic method (0.8 mL min^{-1}) that consisted of 10 % water and 90 % acetonitrile. The detection wavelength was 254 nm. Before irradiation, the mixed solution was allowed to stir in dark for 15 min to achieve gas-liquid equilibrium. The radical scavengers of isopropanol (IPA, 200 mM), furfuryl alcohol (FFA, 1 mM), p-benzoquinone (BQ, 30 mM) and sorbic acid (SA, 5 mM) were added to different systems to scavenge •OH, $^1O_2$, $O_2^{\bullet -}$ and the excited state, respectively (Gao et al., 2020). The concentration of these scavengers was selected according to our previous experiments to ensure that the active species in the system were fully captured. Considering the effect of O_2 on the photochemical degradation of tonalide, the system was continuously aerated for 20 min using N_2 before the photochemical degradation experiments. Each experiment was repeated at least twice to ensure the reproducibility of the results.

2.2.2. Laser flash photolysis (LFP)

Time-resolved transient absorption spectra and transient decay traces were recorded on LKS80 laser flash photolysis (Applied Photophysics Ltd., the United Kingdom) with 266 nm Nd:YAG laser. The laser energy of around 150 mJ was applied in the laser flash photolysis experiments, whereas the pulse duration was 6–7 ns. After laser irradiation of the solution in the 10 × 10 × 40 mm^3 quartz cell, the orthogonal detection light source for 150 W xenon lamp was immediately taken through the sample

cuvette to monochromator equipped with an R955 photomultiplier. The variation of optical signal was transferred to computer for further analysis using HP 54510 B digital oscillograph. The samples were prepared freshly before each test, and high-purity N_2 was bubbled for 20 min to remove dissolved O_2. Besides, all the experiments were conducted at the controlled temperature of 25 °C.

2.2.3. Electron paramagnetic resonance (EPR)

The Bruker EMXPlus-10/12 EPR spectrometer was used to detect and record the electron paramagnetic resonance (EPR) spectra. Detailed instrument parameters and the testing methods are described in Text S2 in SI.

2.3. Identification of the by-products and the prediction of bioaccumulation

For analysis and identification of the degradation by-products, the degradation solution of ATHN was separated using Agilent 1290 HPLC that was equipped with Eclipse plus C_{18} column (1.8 μm, 3 × 150 mm^2) with the flow rate of 0.2 mL min^{-1}. The by-products were qualitatively analyzed using quadrupole time-of-flight (Q-TOF-MS) high-resolution mass spectrometer (Agilent 6545) with the electrospray ionization (ESI) source in positive modes. The temperature of the column was 30 °C. The gradient elution started with 50 % water, 2 ‰ formic acid and 50 % ACN, and 54 % ACN at 8 min. After 7 min, the proportion of ACN was changed to 55 %, and at 20 min, to 60 % ACN. Moreover, at 40 and 47 min, the proportions were changed to 62 % ACN and 70 % ACN, respectively. Their ratio returned to their original values in 1 min and held for 2 min. The entire elution time was 50 min. The optimized mass spectrometry conditions are presented in Text S3 in SI.

The components of tonalide solution at different degradation times were further separated using ZORBAX SB-C_{18} column (5 μm, 9.4 × 150 mm) with the flow rate of 1 mL min^{-1}. The detection wavelength was 254 nm. The mobile phase consisted of water and ACN. The gradient elution started with 60 % ACN, changed linearly to 70 % at 20 min, and to 75 % and 95 % at 50 and 60 min, respectively. Subsequently, the composition of ACN was returned to 60 % in 10 min. Each sample was collected with Agilent 1260 semi-preparative HPLC and was further freeze-dried. The collected samples were redissolved with dimethyl sulfoxide-D6 for NMR analysis. Both the ^{1}H and ^{13}C NMR spectra were recorded using Bruker spectrometer with 600 MHz. Each separated component was verified using HPLC-Q-TOF-MS. All NMR data were processed using MestReNova v 14.1.0 software.

The bioaccumulation risk of tonalide and its photochemical degradation by-products were theoretically estimated using the regression-based method BCFBAF v 3.01 as described in one of our earlier studies (Gao et al., 2016).

3. Results and discussion

3.1. Photochemical degradation kinetics of tonalide

Direct photochemical degradation of tonalide in aquatic environment is possible since tonalide weakly absorbs light that is overlapped (290–310 nm, Fig. S1) with sunlight reaching the Earth's surface (λ > 290 nm). In the control experiment (Fig. S2), only a little loss of tonalide was observed (<1 %), proving that the photochemical degradation of tonalide was nearly negligible without UV irradiation. In contrast, approximately 90 % of tonalide (500 μM) was photochemically degraded within 20 min under UV irradiation (Fig. 1). Moreover, the photochemical degradation kinetics curve of tonalide obeyed the pseudo-first-order kinetic equation (inset of Fig. S2) with apparent rate constant of 24.1 × 10^{-2} min^{-1} (R^2 = 0.99) and the half-life of 2.88 min. These results suggested that UV irradiation can efficiently remove tonalide from water, which is in agreement with many previous studies (Godayol et al., 2015; Santiago-Morales et al., 2013; Santiago-Morales et al., 2012). However, during rapid photochemical degradation, tonalide is inevitably transformed into a variety of by-products. Therefore, it is necessary to further analyze the by-products originating from the photochemical transformation of tonalide and explore the photochemical degradation mechanism of tonalide to better understand its environmental fate.

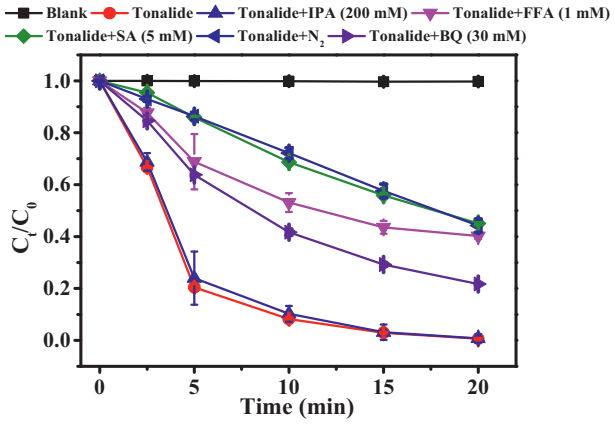

Fig. 1. Tonalide (500 μM) photochemical degradation in the dark and under high pressure mercury lamp with scavenger for 200 mM IPA, 1 mM FFA, 5 mM SA, 30 mM BQ and N_2 saturated; respectively, C_t and C_0 stand for the tonalide concentration at time t and initial tonalide concentration, respectively.

3.2. Photochemical degradation mechanism of tonalide

3.2.1. Identification of photochemical degradation by-products

In order to better understand the photochemical degradation mechanism and the pathway of tonalide, high-performance liquid chromatography quadrupole-time of flight tandem mass spectrometry (HPLC-Q-TOF-MS) was employed to qualitatively identify all the degradation by-products. Under these chromatographic conditions, a total of eight by-products were separated and labeled as peaks P1–P8, as seen in Fig. 2A. Moreover, their retention times, molecular structures, and their confidence levels are listed in Table S1 according to Schymanski scale (Schymanski et al., 2014). As seen in Fig. 2B, the by-products of P2, P3, and P4 appeared as the first-generation degradation by-products. Their peak areas first increased, and then, decreased slowly. Correspondingly, P1, P5, P6, P7 and P8 were identified as the second-generation degradation by-products and increased gradually during the photochemical degradation. Meanwhile, the tonalide concentration continuously decreased.

According to the peak area of by-products, the yield of P1 could be calculated by the ratio of P1 peak area to the sum of peak areas of all the

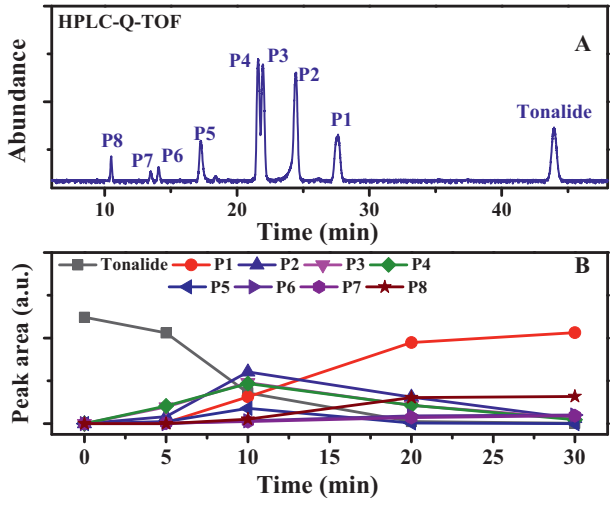

Fig. 2. The total ion current (A) and the peak area (B) of the photochemical degradation by-products of tonalide at different time.

by-products at different time periods. Because the yield of P1 reached up to 65 % within 30 min (Fig. S3), P1 emerged as the main by-product during the photochemical degradation of tonalide. Due to this reason, P1 was first analyzed. As for the degradation by-product, P1 had the *m/z* of 273.1856 and corresponded to $C_{18}H_{24}O_2$ (Fig. S4). Compared with the ^1H NMR spectrum of its parent tonalide (Fig. S5), P1 displayed a pivotal quartet for one H with the chemical shift of 5.60 ppm, implying that O was on the adjacent C of P1 (Fig. S6). Therefore, P1 was rationally identified as the tonalide-lactone. Besides, a corresponding result was also confirmed by its ^{13}C NMR spectrum with the chemical shift at 77.89 ppm (Fig. S6). The critical carbonyl group assigned to the characteristic chemical shift was around 170 ppm. Moreover, according to the molecular structure, the C at 77.89 ppm was deemed to chiral center, while other carbons came in pairs with a 3:2 diastereomeric mixture, as shown in Fig. S6.

The by-products of P2, P3, and P4 were found to be isomers, had the same molecular ion $[M + H]^+$ at the *m/z* of 273.1856 and determined to be $C_{18}H_{24}O_2$ through the HPLC-TOF-MS (Fig. S4). With regards to the analysis of the fragment ions for P2, the m/z of 255.1755 was assigned to $[M + H\text{-}H_2O]^+$. As shown in Fig. S7, the ^1H NMR shift data for two aromatic H and eighteen alkyl H of P2 matched with that of the parent tonalide (Fig. S5). The H within the chemical shift range of 4.80–4.90 showed a key correlation to two methylene groups on pyran, and allowed for the complete structural assignment of P2. However, since P3 and P4 cannot achieve complete separation by chromatography, the isolation and concentration procedure would merge P3 and P4 for the analysis. As shown in Fig. S8, the ^1H NMR spectrum of P3 and P4 displayed twenty-one H on the alkyl group with the chemical shift range of 0.5–3 ppm and two H on the benzene ring at 7.76 and 7.85 ppm. A typical H was observed with the chemical shift of 10.01 ppm and indicated the formation of an aldehyde group for the photochemical degradation by-products. Another evidence to confirm the structure of P3 and P4 was the fragment ion with the *m/z* of 43.0183, which was produced by the fracture of aldehyde group ($[CH_3CO]^+$) though ionization and observed using HPLC-Q-TOF-MS (Fig. S4).

Other secondary by-products of P5, P6, P7 and P8 were analyzed based upon the molecular ion $[M + H]^+$ of 257.1896, 289.1796, 275.1646 and 273.1856, and corresponded to $C_{18}H_{24}O$, $C_{18}H_{24}O_3$, $C_{17}H_{22}O_3$, and $C_{18}H_{24}O_2$, respectively (Fig. S4). Unfortunately, P6, P7 and P8 with the low yield rate could not be completely collected, and the identification of these three by-products was unsuccessful, as observed from the NMR spectrum. The molecular composition of P5 ($C_{18}H_{24}O$) suggested the elimination of two hydrogen atoms from the parent tonalide. With the perfect match of the chemical shift of H on parent tonalide, the structure of tetrahydronaphthalene was still stable in the photochemical degradation by-products (Fig. S9). Besides, four H with two values of chemical shifts at 2.71 and 3.01 ppm for P5 were attributed to the H on cyclopentanone, implying that the structure of indanone was formed (Fig. S9).

Based on the identification of degradation by-products and the validation using custom-prepared standard substances, the molecular structures of these by-products clearly indicated that the photochemical degradation of AHNT mainly occurred on its ketone moiety. These results suggested that ketone moiety was the key active functional group during the photochemical degradation of tonalide. Besides, the formation of tonalide-lactone and other by-products implied the generation of reactive species in the system, which were involved in the photochemical degradation of tonalide. Therefore, to find out the formation mechanism of these by-products and the photochemical degradation pathway of tonalide, a series of reactive species of experiments was conducted to recognize the byproducts.

3.2.2. Recognition of the reactive species during tonalide's photochemical degradation

In general, the photochemical degradation of EOCs is usually caused by various reactive species, such as hydroxyl radicals (•OH), singlet oxygen ($^1O_2$), superoxide anion ($O_2^{\bullet-}$) and excited triplet (Wan et al., 2020; Wang et al., 2015). Therefore, the photochemical degradation kinetics of tonalide with and without scavengers of reactive species (IPA for •OH, FFA for $^1O_2$, BQ for $O_2^{\bullet-}$, and SA for excited triplet) are summarized in Fig. 1 and Table S2, respectively. The degradation efficiency with the addition of isopropanol (IPA) resulted in a reduction of <3 %, indicating that •OH-initiated transformation process did not exert significant effect on the photochemical degradation of tonalide. With the addition of sorbic acid (SA) to capture the triple excited state of tonalide (^{3}tonalide*) in the system, the apparent rate constant decreased from 24.1×10^{-2} to $4.2 \times 10^{-2}\,min^{-1}$, suggesting that 45.4 % of degradation efficiency was contributed by ^{3}tonalide*. When the reactive oxygen $^1O_2$ and $O_2^{\bullet-}$ were captured by furfuryl alcohol (Pan et al., 2015) and p-benzoquinone (BQ) (Li et al., 2018a), the apparent rate constant of $24.1 \times 10^{-2}\,min^{-1}$ was notably suppressed to 3.9×10^{-2} and $6.9 \times 10^{-2}\,min^{-1}$, respectively, indicating that $^1O_2$ and $O_2^{\bullet-}$ contributed to 40.5 % and 21.8 %, respectively. Furthermore, the bubbling of N_2 in the system confirmed the above-mentioned results, and the apparent rate constant of tonalide decreased from 24.1×10^{-2} to $5.3 \times 10^{-2}\,min^{-1}$ with 44.5 % of degradation efficiency coming from ^{3}tonalide* and $^1O_2$. This was due to the reason that N_2 is an established efficient protectant of ^{3}tonalide*, and can eliminate O_2 interference (Gao et al., 2020; Zhang et al., 2019). In short, all the results suggest that tonalide could absorb UV light to form ^{3}tonalide* along with the photochemically produced $^1O_2$ and $O_2^{\bullet-}$, which acted as the initial reactive species to trigger its degradation.

Furthermore, the EPR technology was further used to study the main reactive oxygen species involved in the reaction system. A 1:1:1 triplet signal, characteristic of TEMPO radical with hyperfine splitting constants of $a_N = a_H = 16.7$ G (Fig. 3A), enhanced with the increase in the degradation time, demonstrating that $^1O_2$ was generated in the reaction system according to an early reference (Zhu et al., 2018). However, when DMPO was used as a trapping agent, the results were inconsistent with the expectations, which was a well-known indicator for $^{\bullet}OH$ (in water) and $O_2^{\bullet-}$ (in methanol) (Li et al., 2018a; Zhang et al., 2019). Furthermore, EPR experiments (shown in Fig. 3B) with the addition of scavenger DMPO in methanol exhibited stable signals, which were assigned to DMPO-RO• adduct during the photochemical degradation of tonalide due to the hyperfine splitting constants of $\alpha_N = 13.5$ G and $\alpha_H = 8.8$ G (Azman et al., 2014; Shein and Jeschke, 2019). These results indicated that $O_2^{\bullet-}$ was not produced in the photochemical degradation of tonalide, because the signal of $O_2^{\bullet-}$-DMPO should have six characteristic peaks (Li et al., 2018a). Moreover, it has been reported that, under UV irradiation, acetone could interfere with the generation of $O_2^{\bullet-}$ (Luo et al., 2021). Tonalide has a particular keto structure, which is similar to the characteristic functional group of acetone and indicates that $O_2^{\bullet-}$ was not produced in the system. Besides, BQ is an electron-rich compound, which is not only an effective trapping agent for $O_2^{\bullet-}$, but also acts as an electron shuttle agent (Lan et al., 2022). Therefore, the inhibition of tonalide's photochemical degradation by BQ could be the cause of electron transfer.

Furthermore, as shown in Fig. 3C, two diastereomeric DMPO-RO• adducts were observed in the system of DMPO in water though the hyperfine splitting constants of: $\alpha_N = 14.1$ G, $\alpha^{\beta}_H = 9.2$ G and $\alpha^{\gamma}_H = 1.5$ G and $\alpha^{\delta}_N = 13.7$ G, $\alpha_H = 15.2$ G. These results further reconfirmed that •OH was not involved in the photochemical degradation of tonalide (Zhang et al., 2019). These signals could be similar to those of the adducts for DMPO with polyunsaturated fatty acid, as reported in a previous work (Dikalov and Mason, 2001).

Overall, the above results suggested that a new oxygenated free radical was formed and played an important role in the photochemical degradation of tonalide, while $^1O_2$ could be produced and involved in the photochemical degradation of tonalide. Moreover, it could be speculated that the formation of this new oxygenated radical was due to the photochemical transformation of tonalide triplet rather than the adducts of tonalide and oxygen, which should have formed peroxide according to previous work (Baptista et al., 2017). Therefore, the identification of new oxygenated radicals, as conducted in the current work, facilitates a better understanding of the reaction mechanism of the photochemical degradation of tonalide.

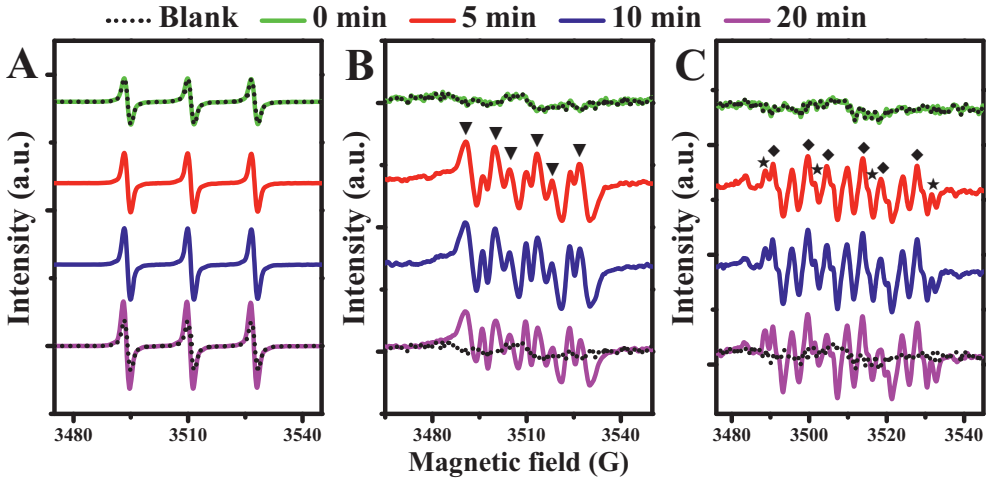

Fig. 3. EPR spectra for TEMP as spin trapping agent in H_2O (A), and EPR spectra DMPO as spin trapping agent in MeOH (B) and H_2O (C) systems. The symbols of ▼ (α_N = 13.5 G and α_H = 8.8 G), ★ (α^{δ}_N = 13.7 G, α_H = 15.2 G) and ◆ (α_N = 14.1 G, α^{β}_H = 9.2 G, α^{γ}_H = 1.5 G) represented as DMPO-RO• adduct.

3.2.3. Transient intermediates formed during the photochemical degradation of tonalide

The LFP is also an effective method to study the reaction mechanism of initial intermediates (Wan et al., 2021). The method was further applied to investigate the initial excited state of tonalide during the photochemical degradation of tonalide (Fig. 4). To get rid of O_2, the transient absorption spectra were obtained after the excitation of tonalide at 266 nm laser under N_2 saturation conditions (Fig. 4A). An asynchronous absorption signal with two absorption bands at 300–450 nm and 650–900 nm was observed at nanoseconds time-resolved scales. Obvious absorption took 4 ns to happen at 760 and 830 nm, and increased with the progression of time. A strong, long-band and structure-free maximum absorption peak at 780 nm was obtained at 12 ns. After 40 ns, higher and stronger absorption peaks appeared at 340 and 390 nm. Comparative analysis of transient absorption in the presence of O_2 showed that a weak absorption peak got enhanced at 520 nm at 8 ns (Fig. 4B), which was assigned to an initial tonalide radical cation (tonalide$^{\bullet+}$) intermediate and resulted from the ejection of an electron (photoionization) from a singlet excited state (Säuberlich et al., 1996). However, the peak at 520 nm disappeared after 20 ns, suggesting that the short-lived tonalide$^{\bullet+}$, and not the oxygenated radicals, could also decay soon.

Incomplete quenching of absorption bands at 300–450 nm and 650–900 nm in the presence of O_2 suggested that the absorption spectrum might be dominated by a superposition of ^{3}tonalide* and oxygenated radicals. Therefore, subtracting the radical background of 100 ns in the O_2-containing sample from that of the overall absorption of 100 ns in N_2-containing sample resulted in a separation of the spectrum of ^{3}tonalide*, which exhibited significant absorption peaks at 340, 390, and 740 nm with a shoulder at 780 nm (Fig. 4C). Moreover, according to the observation of similar transient spectra of various structural analogues, this strong, asynchronous, and near-infrared absorption band centered at 780 nm was consistent with the typical characteristic band of the encounter complex ([^{3}tonalide*]$_{ec}$). The [^{3}tonalide*]$_{ec}$ was a complex formed by the combination of ^{3}tonalide* before it underwent electron transfer to the ion pairs (Rathore et al., 1997). This indicates that ^{3}tonalide* could act as both the electron donor and the electron acceptor in the excited state through [^{3}tonalide*]$_{ec}$. Based on this conclusion, the transient absorption at 340 and 390 nm was attributed to intermolecular hydrogen abstraction intermediate by ^{3}tonalide*, which could result in electron transfer (ortho methyl to acetyl) followed by the generation of a pivotal intermediate triple bi-radicals (340 nm, τ = 83.3 ns) and further yield of photoenol (390 nm, τ = 233 ns). In addition, the transient decays at 340 and 390 nm in N-hexane confirmed these results. Moreover, significantly suppressed and accelerated decay curves were obtained by the inhibition of the dissociation of [^{3}tonalide*]$_{ec}$ by non-polar solvent (Fig. 5A and B), which agreed well with the results reported in previous work (Rathore et al., 1997). From

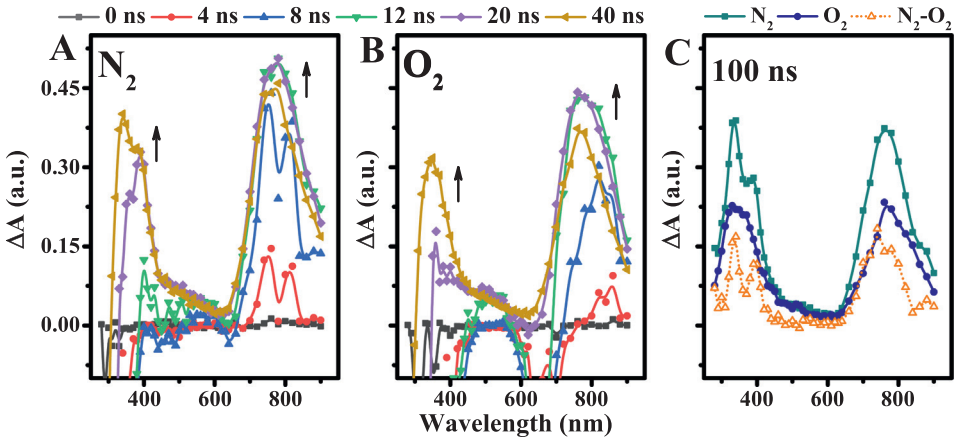

Fig. 4. The LFP scan spectra of tonalide using 266 nm laser: purged with N_2 (A) and O_2 (B), and the spectrum shown by open triangle was obtained from the difference between spectra of 100 ns in the N_2- or O_2-containing sample (C).

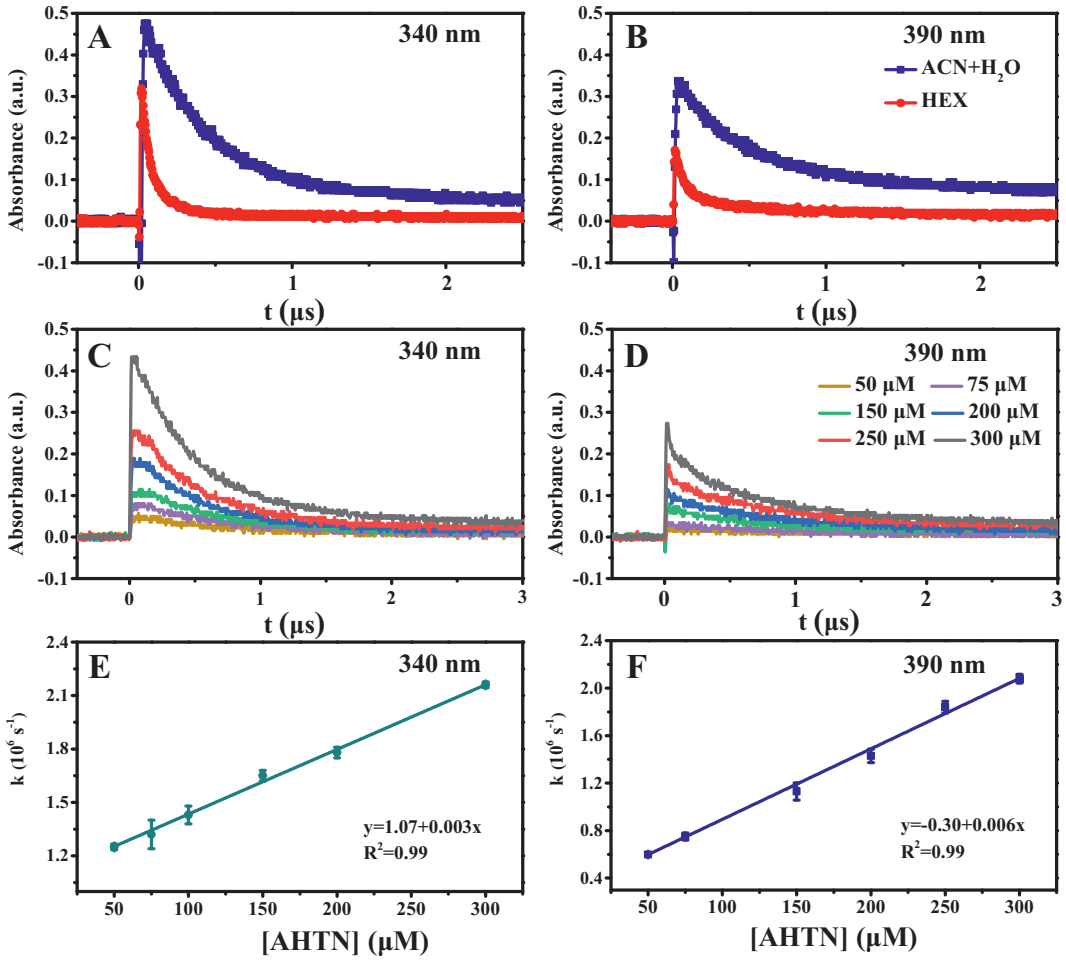

Fig. 5. Decay dynamics of absorption at 340 (A, C), and 390 (B, D) nm obtained after nanosecond laser photolysis of different solvents (A, B) and different tonalide concentrations (C, D). Plot of observed absolute rate constants (k_{obs}) *vs.* tonalide concentrations at 340 (E) and 390 (F) nm.

the linear dependence of the intensities of these peaks on the concentration of tonalide (Fig. 5C–F), the values for the absolute decay rate constants at 340 and 390 nm were determined to be $3.61 \pm 0.01 \times 10^9\ M^{-1}\ s^{-1}$ and $6.31 \pm 0.01 \times 10^9\ M^{-1}\ s^{-1}$, respectively. These results indicated that the formation of bi-radicals was the key step during the photochemical degradation of tonalide.

In comparison to other direct photochemical degradation processes, the carbonyl group of EOCs is usually the center of the photochemical reactivity. For instance, under UV irradiation, the photochemical transformation of salinomycin and narasin could result in the photochemical cleavage on the carbonyl group (Sun et al., 2014b). The carbonyl oxygen of ketones can undergo enol-keto tautomerization to yield photoenols (Klán et al., 2013; Sebej et al., 2011), which has been reported by the photochemical degradation of organic pollutants (Wang et al., 2015). Surprisingly, in this study, a new interesting organic free radical, the bi-radicals of the photoenol precursors, were detected for the first time during the photochemical degradation of tonalide. Although bi-radicals have also been reported during the photochemical degradation of triclosan, it was difficult to match both the conditions, preferential exposure of phenoly-oxygen anions (pH > 7) and dichlorination (Kliegman et al., 2013). However, tonalide could result in intermolecular H-abstraction reaction due to the encounter complex of $[^3\text{tonalide}*]_{ec}$ to generate bi-radicals, yielding photoenol, for which an additional deionization process was not required. The possible processes of photochemical degradation of tonalide could be summarized by Eqs. (1)–(4).

$$\text{tonalide} \xrightarrow{h\nu} {}^1\text{tonalide}^* \xrightarrow{ISC} {}^3\text{tonalide}^* \quad (1)$$

$$^3\text{tonalide}^* + O_2 \rightarrow \text{tonalide} + {}^1O_2 \quad (2)$$

$$^3\text{tonalide}^* \rightarrow [^3\text{tonalide}^*]_{ec} \xrightarrow{\text{Hydrogen transfer}} \text{Bi}-\text{radicals} \quad (3)$$

$$\text{Bi}-\text{radicals} \xrightarrow{\text{Photoenolization}} \text{Photoenols} \quad (4)$$

3.2.4. Photochemical degradation pathway of tonalide

During the photochemical degradation of tonalide, a process of continuous photoenolization is proposed tentatively as shown in Scheme 1. The pathway is based upon the above results about the recognition of reactive species, the observation of transient intermediates and the identification of eight degradation by-products. During Step 1, initially, the excited singlet state of tonalide (^{1}tonalide∗) was formed under UV irradiation, and then, transformed to ^{3}tonalide∗. Furthermore, ^{3}tonalide∗ underwent intramolecular 1,5-hydrogen abstraction reaction to form bi-radicals. Meanwhile, the formation of encounter complex ($[^3\text{tonalide}*]_{ec}$) became favorable for the generation of bi-radicals. During Step 2, the bi-radicals sequentially yielded photoenol, whereas P5 was generated *via* the cyclization of photoenol (Park and Ryu, 2010). Moreover, photoenol could also revert to parent tonalide *via* fast 1,5-sigmatropic hydrogen transfer reaction (Klán et al., 2013; Pelliccioli et al., 2012). Furthermore, the formation of P5 was completely suppressed under O_2 saturation due to the competition of the reaction of bi-radicals with O_2 (Fig. S10). Therefore, the delocalization of bi-radicals reacted with O_2 to form peroxide intermediate 1 or 2, which was followed by the rearrangement and ring-opening reactions to generate P3 and P4. During Step 3, with the production of new alkylphenyl ketones,

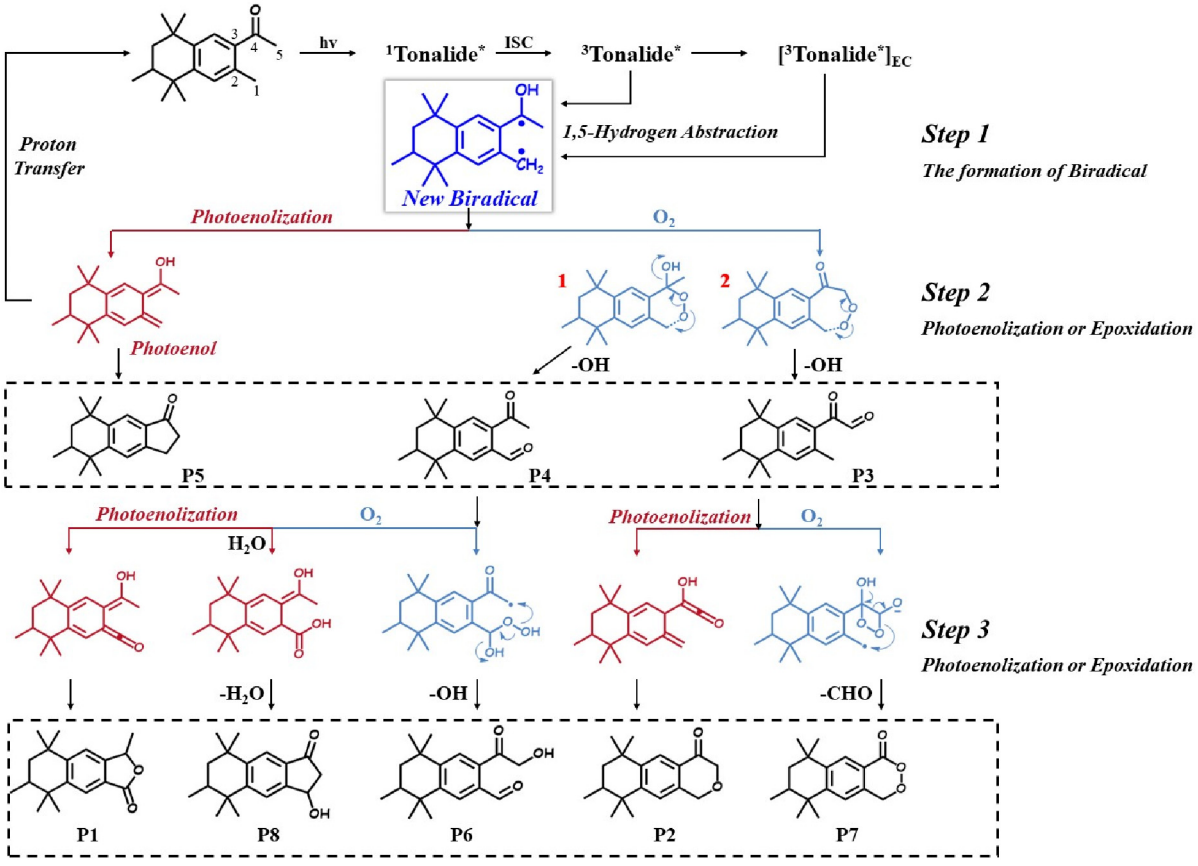

Scheme 1. Proposed transformation pathways for tonalide photolysis. P1 (3,5,5,7,8,8-hexamethyl-5,6,7,8-tetrahydronaphtho[2,3-*c*]furan-1(3H)-one), P2 (6,6,8,9,9-pentamethyl-6,7,8,9-tetrahydro-1H-benzo[*g*]isochromen-4(3H)-one), P3 (2-(3,5,5,6,8,8-hexamethyl-5,6,7,8-tetrahydronaphthalen-2-yl)-2-oxoacetaldehyde), P4 (3-acetyl-5,5,7,8,8-pentamethyl-5,6,7,8-tetrahydronaphthalene-2-carbaldehyde), P5 (5,5,6,8,8-pentamethyl-2,3,5,6,7,8-hexahydro-1H-cyclopenta[*b*]naphthalen-1-one), P6 (3-(2-hydroxyacetyl)-5,5,7,8,8-pentamethyl-5,6,7,8-tetrahydronaphthalene-2-carbaldehyde), P7 (6,6,7,9,9-pentamethyl-6,7,8,9-tetrahydronaphtho[2,3-d][1,2]dioxin-1(4H)-one), P8 (3-hydroxy-5,5,6,8,8-pentamethyl-2,3,5,6,7,8-hexahydro-1H-cyclopenta[*b*]naphthalen-1-one).

the intramolecular 1,5-hydrogen abstraction happened from P3 and P4 to form P1 and P2, respectively. On the other hand, the bi-radical species from P3 and P4 could further react with O_2 with the rearrangement and ring-opening reaction to form P6 and P7. Notably, the formation of P8 was depressed in the dehydrated solvents (Fig. S10), indicating that solvent water participated during the formation of P8. A similar process was reported in an earlier study (Park and Ryu, 2010; Plíštil et al., 2006). This means that the solvent water was added to the triplet state of aldehyde group through proton exchange and formed a bi-radical intermediate. Therefore, P8 was generated from the nucleophilic addition of H_2O followed by the photoenolization of bi-radicals.

Briefly speaking, the photochemical degradation of tonalide could first generate bi-radicals, which sequentially yielded photoenol. Further pathway of photochemical degradation of tonalide could occur through continuous photoenolization followed by cyclization with O_2 to form various by-products. Moreover, the bi-radicals were generated due to the electron transfer between the aromatic ketones and alkyl substituents. These results imply that the same mechanism could exist in synthetic musks with similar structures. These findings advance the knowledge of photochemical degradation and the environmental fate of synthetic musks.

3.3. Bioaccumulation risk assessment of tonalide and key by-products

In order to quickly screen the toxicity of tonalide and its photochemical degradation by-products, acute and chronic toxicities to fish were employed using the ECOSAR program. According to the aquatic toxicity criteria of the European Union (shown in Fig. S13), despite a potential decreasing toxicity risk during the photochemical degradation of tonalide, tonalide and its by-products were identified to be toxic. The detailed analysis is described in Text S4 in SI. However, the high concentration of tonalide in aquatic organisms has been documented in previous work (Wan et al., 2007), indicating potential bioaccumulation of the tonalide. It is necessary to assess the bioaccumulation effects of tonalide with aquatic toxicity. Therefore, to further investigate whether the by-products formed through photoenolization during the photochemical degradation of tonalide had the potential of bioaccumulation or not, and whether they bioaccumulated more strongly than the parent tonalide, the bioconcentration factors (BCF) of tonalide as well as the key degradation by-products were evaluated using computational toxicology.

According to the range of promulgated bioaccumulation (Gao et al., 2016), the value of $1 < BCF < 1000$ L/kg wet-wt was regarded as having the "tendency to accumulate in organisms", whereas the values of $1000 < BCF < 5000$ and $BCF > 5000$ L/kg wet-wt belonged to the levels of "bioaccumulative" and "very bioaccumulative", respectively. These results of bioaccumulation assessment are shown in Fig. S11. The BCF of tonalide was obtained as 696 L/kg wet-wt and was consistent with the experimental data for zebrafish (600 L/kg wet-wt) and Crucian carp (670 L/kg wet-wt) (Gao et al., 2016), indicating the reliability of computational toxicology and showing that tonalide has a significant bioaccumulation potential with high BCF value. However, according to the transformation pathway, it was surprising to find that the BCF of key degradation by-product, photoenol, was obtained as "very bioaccumulative" with the value of 9515 kg wet-wt, which was 13.6 times higher than that of the tonalide. This value tremendously exceeded the standard threshold (5000 kg wet-wt) set of the typical persistent organics, and therefore, is termed as critically bioaccumulative according to the standard outlined in an earlier

work (Gao et al., 2016). With the further decay and degradation, photoenol would be reverted to the parent tonalide and cyclized to form P5 with BCF of 1560 kg wet-wt. With this BCF, it was considered to be "bioaccumulative" and was still more accumulative than tonalide. Moreover, another two by-products (P1 and P3) were also found to have the BCF of 1360 and 1560 L/kg wet-wt. Both of them were classified as "bioaccumulative". Notably, comparing with tonalide, tonalide-lactone (P1) might be more photostable due to the slower photochemical degradation rate (Fig. S12), indicating their high occurrence in the aquatic environment. As seen in Fig. S11, although the lower bioaccumulation factors were observed for many other degradation by-products (P2, P4, P6, P7, and P8), the health risk of all these by-products may still be believed as having the potential to bioaccumulate in fish and therefore, cannot be ignored. These theoretical results successfully revealed that aquatic organisms might suffer more severe effects from these by-products than that of tonalide due to the formation of these by-products with increased BCFs.

As mentioned earlier, tonalide was readily degraded by forming key bi-radicals upon photochemical irradiation. These bi-radicals were further converted into by-products that were toxic to aquatic organisms. Therefore, the formation of bi-radicals could be used to better understand the formation mechanism and environmental fate of these toxic by-products, showing potential harm to aquatic organisms in the aqueous environment.

4. Conclusions

This work mainly investigated the photochemical degradation kinetics and mechanism of typical synthetic musks, tonalide. Based on results obtained about the reactive species and the identification of degradation by-products, the fate and bioaccumulation risk of tonalide in aquatic environment were revealed. The main conclusions are drawn as follows.

1) Rapid photochemical degradation of tonalide was observed within 20 min. The pseudo-first-order kinetics with apparent rate constant of 0.24 min^{-1} and the half-life of 2.88 min described the photochemical degradation of tonalide.
2) The precise structures of the photochemical degradation by-products of tonalide were identified through the analysis of HPLC-Q-TOF-MS and further validated using NMR analysis on custom-synthesized standard samples.
3) A critical free radical, the bi-radical, was found in the photochemical degradation of tonalide for the first time. The special bi-radicals came from the intramolecular 1,5-hydrogen abstraction reaction of ^{3}tonalide*. In addition, the typical transient absorption peak for this bi-radical at 340 nm was observed using LFP, and the absolute decay rate constant at 340 nm was determined to be $3.61 \pm 0.01 \times 10^{9}$ $M^{-1}\ s^{-1}$.
4) Continuous photoenolization was proposed to yield photoenol. Additionally, the former species will convert efficiently back to the parent tonalide and cyclized to form other by-products.
5) The bioconcentration factor of the photoenol was 13-fold higher than that of tonalide, indicating that the bioaccumulation risk of photoenol to aquatic organisms may even be severer than that of tonalide.

CRediT authorship contribution statement

Na Luo: Methodology, Formal analysis, Writing - original draft.
Yanpeng Gao: Methodology, Data curation.
Mei Wang: Visualization, Investigation.
Xiaolin Niu: Investigation.
Guiying Li: Writing - Reviewing and Editing.
Taicheng An: Conceptualization, Supervision, Editing.

Data availability

No data was used for the research described in the article.

Declaration of competing interest

The authors declare that they have no known competing financial interests or personal relationships that could have appeared to influence the work reported in this paper.

Acknowledgements

This work was supported by National Key Research and Development Program of China (2019YFC1804503 and 2019YFC1804501), Local Innovative and Research Teams Project of Guangdong Pearl River Talents Program (2017BT01Z032), Key-Area Research and Development Program of Guangdong Province (2020B1111350002), National Natural Science Foundation of China (41977365 and 41425015).

Appendix A. Supplementary data

Supplementary data to this article can be found online at https://doi.org/10.1016/j.scitotenv.2022.160311.

References

Azman, N.A.M., Peiro, S., Fajari, L., Julia, L., Almajano, M.P., 2014. Radical scavenging of white tea and its flavonoid constituents by electron paramagnetic resonance (EPR) spectroscopy. J. Agric. Food Chem. 62, 5743–5748.
Baptista, M.S., Cadet, J., Di Mascio, P., Ghogare, A.A., Greer, A., Hamblin, M.R., et al., 2017. Type I and type II photosensitized oxidation reactions: guidelines and mechanistic pathways. Photochem. Photobiol. 93, 912–919.
Dikalov, S.I., Mason, R.P., 2001. Spin trapping of polyunsaturated fatty acid-derived peroxyl radicals: reassignment to alkoxyl radical adducts. Free Radic. Biol. Med. 30, 187–197.
Fang, H., Li, G., Yao, S., Liang, X., An, T., 2017. Kinetic and mechanism studies of musk tonalide reacted with hydroxyl radical and the risk assessment of degradation products. Catal. Today 281, 642–648.
Gao, Y., Ji, Y., Li, G., Mai, B., An, T., 2016. Bioaccumulation and ecotoxicity increase during indirect photochemical transformation of polycyclic musk tonalide: a modeling study. Water Res. 105, 47–55.
Gao, Y., Niu, X., Qin, Y., Guo, T., Ji, Y., Li, G., et al., 2020. Unexpected culprit of increased estrogenic effects: oligomers in the photodegradation of preservative ethylparaben in water. Water Res. 176, 115745.
Gao, Y., Niu, X., Wang, M., Li, G., An, T., 2021. An inescapable fact: toxicity increase during photo-driven degradation of emerging contaminants in water environments. Curr. Opin. Green Sustain. 30, 100472.
Godayol, A., Gonzalez-Olmos, R., Sanchez, J.M., Anticó, E., 2015. Assessment of the effect of UV and chlorination in the transformation of fragrances in aqueous samples. Chemosphere 125, 25–32.
Hu, Z., Shi, Y., Cai, Y., 2011. Concentrations, distribution, and bioaccumulation of synthetic musks in the Haihe River of China. Chemosphere 84, 1630–1635.
Jiang, P., Qiu, J., Gao, Y., Stefan, M.I., Li, X.F., 2021. Nontargeted identification and predicted toxicity of new byproducts generated from UV treatment of water containing micropollutant 2-mercaptobenzothiazole. Water Res. 188, 116542.
Klán, P., Solomek, T., Bochet, C.G., Blanc, A., Givens, R., Rubina, M., et al., 2013. Photoremovable protecting groups in chemistry and biology: reaction mechanisms and efficacy. Chem. Rev. 113, 119–191.
Kliegman, S., Eustis, S.N., Arnold, W.A., McNeill, K., 2013. Experimental and theoretical insights into the involvement of radicals in triclosan phototransformation. Environ. Sci. Technol. 47, 6756–6763.
Lan, T., Wu, P., Liu, Z., Stroet, M., Liao, J., Chai, Z., et al., 2022. Understanding the effect of pH on the solubility and aggregation extent of humic acid in solution by combining simulation and the experiment. Environ. Sci. Technol. 56, 917–927.
Lee, I.S., Lee, S.H., Oh, J.E., 2010. Occurrence and fate of synthetic musk compounds in water environment. Water Res. 44, 214–222.
Li, B., Lai, C., Zeng, G., Qin, L., Yi, H., Huang, D., et al., 2018a. Facile hydrothermal synthesis of Z-scheme Bi2Fe4O9/Bi2WO6 heterojunction photocatalyst with enhanced visible light photocatalytic activity. ACS Appl. Mater. Interfaces 10, 18824–18836.
Li, X., Chu, Z., Yang, J., Li, M., Du, M., Zhao, X., et al., 2018b. Synthetic musks: a class of commercial fragrance additives in personal care products (PCPs) causing concern as emerging contaminants. Adv. Mar. Biol. 81, 213–280.
Liu, N., Shi, Y., Xu, L., Li, W., Cai, Y., 2013. Occupational exposure to synthetic musks in barbershops, compared with the common exposure in the dormitories and households. Chemosphere 93, 1804–1810.
Liu, J., Zhang, W., Zhou, Q., Zhou, Q., Zhang, Y., Zhu, L., 2020. Polycyclic musks in the environment: a review of their concentrations and distribution, ecological effects and behavior, current concerns and future prospects. Crit. Rev. Environ. Sci. Technol. 51, 323–377.
Luo, Z., Spinney, R., Wei, Z., Hu, W.-P., Villamena, F.A., Song, W., et al., 2021. Reevaluation of the reactivity of superoxide radicals with a sulfonamide antibiotic, sulfacetamide: an experimental and theoretical study. ACS ES&T Water 1, 2339–2347.
Montes-Grajales, D., Fennix-Agudelo, M., Miranda-Castro, W., 2017. Occurrence of personal care products as emerging chemicals of concern in water resources: a review. Sci. Total Environ. 595, 601–614.

Moon, H.B., Lee, D.H., Lee, Y.S., Kannan, K., 2012. Occurrence and accumulation patterns of polycyclic aromatic hydrocarbons and synthetic musk compounds in adipose tissues of korean females. Chemosphere 86, 485–490.
Pan, T.L., Wang, P.W., Aljuffali, I.A., Huang, C.T., Lee, C.W., Fang, J.Y., 2015. The impact of urban particulate pollution on skin barrier function and the subsequent drug absorption. J. Dermatol. Sci. 78, 51–60.
Park, B.S., Ryu, H.J., 2010. Unique solvent effect on photochemistry of ortho-alkylphenacyl benzoates. Tetrahedron Lett. 51, 1512–1516.
Parolini, M., Magni, S., Traversi, I., Villa, S., Finizio, A., Binelli, A., 2015. Environmentally relevant concentrations of galaxolide (HHCB) and tonalide (AHTN) induced oxidative and genetic damage in Dreissena polymorpha. J. Hazard. Mater. 285, 1–10.
Pelliccioli, A.P., Sebej, P., Wirz, J., 2012. Ketonization of enols in aqueous solution: is carbon protonation always rate-determining? Photochem. Photobiol. Sci. 11, 967–971.
Plíštil, L., Šolomek, T., Wirz, J., Heger, D., Klán, P., 2006. Photochemistry of 2-alkoxymethyl-5-methylphenacyl chloride and benzoate. J. Org. Chem. 71, 8050–8058.
Rathore, R., Hubig, S.M., Kochi, J.K., 1997. Direct observation and structural characterization of the encounter complex in bimolecular electron transfers with photoactivated acceptors. J. Am. Chem. Soc. 119, 11468–11480.
Reiner, J.L., Kannan, K., 2006. A survey of polycyclic musks in selected household commodities from the United States. Chemosphere 62, 867–873.
Sanchez-Prado, L., Lourido, M., Lores, M., Llompart, M., Garcia-Jares, C., Cela, R., 2004. Study of the photoinduced degradation of polycyclic musk compounds by solid-phase microextraction and gas chromatography/mass spectrometry. Rapid Commun. Mass Spectrom. 18, 1186–1192.
Santiago-Morales, J., Gomez, M.J., Herrera, S., Fernandez-Alba, A.R., Garcia-Calvo, E., Rosal, R., 2012. Oxidative and photochemical processes for the removal of galaxolide and tonalide from wastewater. Water Res. 46, 4435–4447.
Santiago-Morales, J., Gomez, M.J., Herrera-Lopez, S., Fernandez-Alba, A.R., Garcia-Calvo, E., Rosal, R., 2013. Energy efficiency for the removal of non-polar pollutants during ultraviolet irradiation, visible light photocatalysis and ozonation of a wastewater effluent. Water Res. 47, 5546–5556.
Säuberlich, J., Brede, O., Beckert, D., 1996. Photoionization of benzophenone carboxylic acids in aqueous solution. A FT EPR and optical spectroscopy study of radical cation decay. J. Chem. Phys. 100, 18101–18107.
Schymanski, E.L., Jeon, J., Gulde, R., Fenner, K., Ruff, M., Singer, H.P., et al., 2014. Identifying small molecules via high resolution mass spectrometry: communicating confidence. Environ. Sci. Technol. 48, 2097–2098.
Sebej, P., Lim, B.H., Park, B.S., Givens, R.S., Klan, P., 2011. The power of solvent in altering the course of photorearrangements. Org. Lett. 13, 644–647.
Shein, M., Jeschke, G., 2019. Comparison of free radical levels in the aerosol from conventional cigarettes, electronic cigarettes, and heat-not-burn tobacco products. Chem. Res. Toxicol. 32, 1289–1298.
Sun, P., Casteel, K., Dai, H., Wehmeyer, K.R., Kiel, B., Federle, T., 2014a. Distributions of polycyclic musk fragrance in wastewater treatment plant (WWTP) effluents and sludges in the United States. Sci. Total Environ. 493, 1073–1078.
Sun, P., Pavlostathis, S.G., Huang, C.H., 2014b. Photodegradation of veterinary ionophore antibiotics under UV and solar irradiation. Environ. Sci. Technol. 48, 13188–13196.
Villa, S., Assi, L., Ippolito, A., Bonfanti, P., Finizio, A., 2012. First evidences of the occurrence of polycyclic synthetic musk fragrances in surface water systems in Italy: spatial and temporal trends in the Molgora River (Lombardia Region, Northern Italy). Sci. Total Environ. 416, 137–141.
Vione, D., Carena, L., 2020. The possible production of harmful intermediates is the "dark side" of the environmental photochemistry of contaminants (potentially adverse effects, and many knowledge gaps). Environ. Sci. Technol. 54, 5328–5330.
Wan, Y., Wei, Q., Hu, J., Jin, X., Zhang, Z., Zhen, H., et al., 2007. Levels, tissue distribution, and age-related accumulation of synthetic musk fragrances in Chinese sturgeon (Acipenser sinensis): comparison to organochlorines. Environ. Sci. Technol. 41, 424–430.
Wan, D., Wang, H., Pozdnyakov, I.P., Wang, C., Su, J., Zhang, Y., et al., 2020. Formation and enhanced photodegradation of chlorinated derivatives of bisphenol A in wastewater treatment plant effluent. Water Res. 184, 116002.
Wan, D., Wang, J., Dionysiou, D.D., Kong, Y., Yao, W., Selvinsimpson, S., et al., 2021. Photogeneration of reactive species from biochar-derived dissolved black carbon for the degradation of amine and phenolic pollutants. Environ. Sci. Technol. 55, 8866–8876.
Wang, L., Liu, X., 2019. Degradation of aqueous polycyclic musk tonalide by ultraviolet-activated free chlorine. Processes 7, 95.
Wang, X., Hu, X., Zhang, H., Chang, F., Luo, Y., 2015. Photolysis kinetics, mechanisms, and pathways of tetrabromobisphenol a in water under simulated solar light irradiation. Environ. Sci. Technol. 49, 6683–6690.
Wang, H., Xi, H., Xu, L., Jin, M., Zhao, W., Liu, H., 2021. Ecotoxicological effects, environmental fate and risks of pharmaceutical and personal care products in the water environment: a review. Sci. Total Environ. 788, 147819.
Yamauchi, R., Ishibashi, H., Hirano, M., Mori, T., Kim, J.W., Arizono, K., 2008. Effects of synthetic polycyclic musks on estrogen receptor, vitellogenin, pregnane X receptor, and cytochrome P450 3A gene expression in the livers of male medaka (Oryzias latipes). Aquat. Toxicol. 90, 261–268.
Zhang, X., Jing, Y., Ma, L., Zhou, J., Fang, X., Zhang, X., et al., 2015. Occurrence and transport of synthetic musks in paired maternal blood, umbilical cord blood, and breast milk. Int. J. Hyg. Environ. Health 218, 99–106.
Zhang, Y., Huang, L., Zhao, Y., Hu, T., 2017. Musk xylene induces malignant transformation of human liver cell line L02 via repressing the TGF-β signaling pathway. Chemosphere 168, 1506–1514.
Zhang, W., Gao, Y., Qin, Y., Wang, M., Wu, J., Li, G., et al., 2019. Photochemical degradation kinetics and mechanism of short-chain chlorinated paraffins in aqueous solution: a case of 1-chlorodecane. Environ. Pollut. 247, 362–370.
Zhu, S., Li, X., Kang, J., Duan, X., Wang, S., 2018. Persulfate activation on crystallographic manganese oxides: mechanism of singlet oxygen evolution for nonradical selective degradation of aqueous contaminants. Environ. Sci. Technol. 53, 307–315.